Editors' Suggestion

Orders of Magnitude Improved Cyclotron-Mode Cooling for Nondestructive Spin Quantum Transition Spectroscopy with Single Trapped Antiprotons

B. M. Latacz,[1,2] M. Fleck,[1,3] J. I. Jäger,[1,2,4] G. Umbrazunas,[1,5] B. P. Arndt,[1,4,6] S. R. Erlewein,[1,4] E. J. Wursten,[1] J. A. Devlin,[1,2] P. Micke,[1,2,4] F. Abbass,[7] D. Schweitzer,[7] M. Wiesinger,[4] C. Will,[4] H. Yildiz,[7] K. Blaum,[4] Y. Matsuda,[3] A. Mooser,[4] C. Ospelkaus,[8,9] C. Smorra,[1,7] A. Soter,[5] W. Quint,[6] J. Walz,[7,10] Y. Yamazaki,[1] and S. Ulmer[1,11]

(BASE Collaboration)

[1]*RIKEN, Ulmer Fundamental Symmetries Laboratory, 2-1 Hirosawa, Wako, Saitama, 351-0198, Japan*
[2]*CERN, Esplanade des Particules 1, 1217 Meyrin, Switzerland*
[3]*Graduate School of Arts and Sciences, University of Tokyo, 3-8-1 Komaba, Meguro, Tokyo 153-0041, Japan*
[4]*Max-Planck-Institut für Kernphysik, Saupfercheckweg 1, D-69117, Heidelberg, Germany*
[5]*Eidgenössisch Technische Hochschule Zürich, Rämistrasse 101, 8092 Zürich, Switzerland*
[6]*GSI-Helmholtzzentrum für Schwerionenforschung GmbH, Planckstraße 1, D-64291 Darmstadt, Germany*
[7]*Institut für Physik, Johannes Gutenberg-Universität, Staudinger Weg 7, D-55099 Mainz, Germany*
[8]*Institut für Quantenoptik, Leibniz Universität, Welfengarten 1, D-30167 Hannover, Germany*
[9]*Physikalisch-Technische Bundesanstalt, Bundesallee 100, D-38116 Braunschweig, Germany*
[10]*Helmholtz-Institut Mainz, Johannes Gutenberg-Universität, Staudingerweg 18, D-55128 Mainz, Germany*
[11]*Heinrich Heine University, Düsseldorf, Univeristätsstrasse 1, D-40225 Düsseldorf, Germany*

(Received 5 July 2023; revised 8 May 2024; accepted 17 June 2024; published 1 August 2024)

We demonstrate efficient subthermal cooling of the modified cyclotron mode of a single trapped antiproton and reach particle temperatures $T_+ = E_+/k_B$ below 200 mK in preparation times shorter than 500 s. This corresponds to the fastest resistive single-particle cyclotron cooling to subthermal temperatures ever demonstrated. By cooling trapped particles to such low energies, we demonstrate the detection of antiproton spin transitions with an error rate $< 0.000\,023$, more than 3 orders of magnitude better than in previous best experiments. This method has enormous impact on multi-Penning-trap experiments that measure magnetic moments with single nuclear spins for tests of matter and antimatter symmetry, high-precision mass spectrometry, and measurements of electron g factors bound to highly charged ions that test quantum electrodynamics and establish standards for magnetometry.

DOI: 10.1103/PhysRevLett.133.053201

Experiments conducted with single particles in Penning traps play a crucial role in achieving ultrahigh precision measurements of masses [1], magnetic moments [2], and fundamental constants [3]. Moreover, they provide stringent tests of the fundamental symmetries of the standard model of particle physics. Penning traps have been instrumental in performing the most precise direct tests of charge-parity-time reversal invariance in both the lepton sector [4] and the baryon sector [5], and in establishing new standards for magnetometry [6]. These traps also enable ultraprecise measurements that test quantum electrodynamics [7–9] and contribute to searches for exotic physics [10,11]. General limitations in precision Penning-trap studies are caused by magnetic field B_0 and electrostatic trap imperfections that lead to particle-energy dependent scaling of the measured cyclotron frequency $\nu_c = (qB_0)/(2\pi m)$ and the spin precession frequency ν_L [5,12], (q/m) is the charge-to-mass ratio of the trapped particle. These energy-dependent frequency shifts impose systematic shifts and uncertainties in the determination of fundamental constants, and limit fractional accuracy. Furthermore, many experiments that employ coherent techniques for measuring cyclotron frequencies of individual trapped particles [13,14] face limitations due to cyclotron energy scatter, which scales proportionally to the thermal phase-space volume of the initial energy distribution before coherent manipulation drives are applied [15]. In the case of directly measuring nuclear magnetic moments such as that of the proton [2], the antiproton [16], or of $^3He^{2+}$, the fidelity

of spin state detection in single-particle quantum transition spectroscopy experiments is constrained by the energy E_+ in the cyclotron mode [17], while employing incoherent quantum-spectroscopy techniques [16]. This necessitates the development of efficient cooling techniques that can reliably achieve particle energies lower than those attained by the commonly used resistive cooling systems in these experiments.

In this manuscript we report on the implementation of a subthermal cooling device, that consists of two stacked Penning traps, a cooling trap (CT) and an analysis trap (AT), and its attached particle manipulation electronics. The CT is equipped with a resonant high-Q resistor-inductor-capacitor circuit, that acts at its resonance as efficient cooling resistor [18] and features high particle-to-detector coupling. The AT has a strong magnetic inhomogeneity superimposed [19], and allows us to determine modified cyclotron energies E_+ with 0.86 μeV resolution in averaging times of ≈10 s. Using this two-trap-device, we successfully demonstrate the preparation of a single trapped antiproton with a cyclotron temperature $T_+ = E_+/k_B$ below 200 mK, which is suitable for quantum-spectroscopy experiments with single antiproton spins with an error rate below $< 0.000\,023$, more than $1500\times$ better than in previous best experiments [20]. The typical preparation time for achieving these conditions is approximately 500 s, which is more than 80× faster compared to our previous experiments [16]. This achievement represents the most rapid cooling of the modified cyclotron mode for single trapped protons and antiprotons reported to date, and has enormous impact on high precision comparisons on then fundamental properties of protons and antiprotons, as well as on magnetic moment measurements of heavier nuclei, such as $^3He^{2+}$.

Our experimental setup involves a superconducting magnet with a horizontal bore, which operates at a magnetic field strength of $B_0 = 1.945$ T. Inside the magnet bore, we have positioned our cryogenic multi-Penning trap system, housed in a hermetically sealed vacuum chamber, in which pressures below 10^{-18} mbar are achieved [21]. For the work reported here, we have extended our multi-Penning trap stack [22] by the CT, and use the AT/CT two-trap system shown in Fig. 1(a). Both traps are in cylindrical five-electrode geometry [23] with an inner electrode diameter of 3.6 mm. A carefully rf-shielded helical resonant cooling resistor [18,24] is connected to a radially segmented correction electrode of the CT. This device is cooled to environmental temperature of ≈ 5 K, and has a varactor-based resonance frequency tuning bandwidth of 4.5 MHz around a center frequency of $\nu_{+,\mathrm{CT}} \approx 28.623$ MHz. To suppress stray-noise pickup of electromagnetic interference and to maximize the system inductance L_{CT}, the cooling resistor is mounted inside the trap vacuum chamber. In thermal equilibrium, the quality factor of the resonant cooling resistor is at $Q \approx 1050(50)$, leading

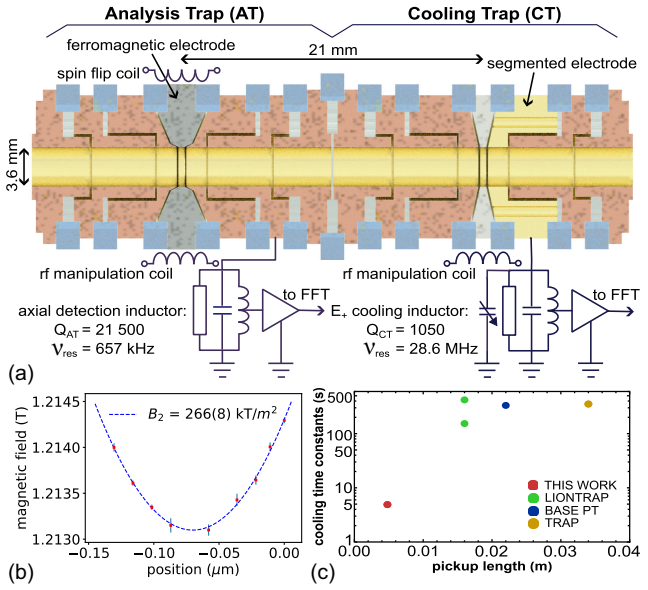

FIG. 1. (a) Double trap system, consisting of a cooling trap (CT) and an analysis trap (AT), with a superimposed magnetic bottle with a strength of $B_{2,\mathrm{AT}} = 266(8)$ kT/m^2. The CT is equipped with a resonant cooling resistor to thermalize the modified cyclotron mode. To the end-cap electrode of the AT an $Q \approx 21\,500$ superconducting detection system at 657 kHz is connected, providing optimum frequency measurement performance at the given trap and detector geometry. (b) Magnetic field in the center of the AT. (c) Comparison of cooling time constants for different trap experiments. Our experiment is operated at $\tau_{+,\mathrm{CT}} \approx 4.5$ s, more than 10× faster than other state-of-the-art trap experiments.

with $L \approx 1.78(3)$ μH to a cooling resistance of $R_{\mathrm{p,CT}} = 2\pi\nu_{+,\mathrm{CT}}QL \approx 340$ kΩ. Once the detector's resonance frequency is tuned to the modified cyclotron frequency of a single trapped (anti)proton, particle-detector interaction thermalizes the modified cyclotron energy E_+ within a correlation time of [25]

$$\tau_{+,\mathrm{CT}} = \frac{m}{R_p}\left(\frac{D_{+,\mathrm{eff}}}{q}\right)^2; \tag{1}$$

here, $D_{+,\mathrm{eff}} = 4.82$ mm is the effective pickup length of the trap at the chosen electrode geometry. By design we expect $\tau_{+,\mathrm{CT,D}} = 4.5(2)$ s, corresponding to a more than 20-fold improvement compared to other state-of-the-art trap experiments [2,13,26], and to an ≈100-fold reduction compared to the performance of our previous antiproton experiments [5,16], see Fig. 1(c).

The magnetic field $B_{\mathrm{AT}}(z) = B_{0,\mathrm{AT}} + B_{2,\mathrm{AT}}z^2$ of the analysis trap has a magnetic bottle with a strength of $B_{2,\mathrm{AT}} = 266(8)$ kT/m^2 superimposed, as shown in Fig. 1(b). The background magnetic field of that trap is $B_{0,\mathrm{AT}} = 1.212$ T. The strong $B_{2,\mathrm{AT}}$ is used for the high-resolution determination of the modified cyclotron energy E_+, reducing the determination of E_+ to a measurement

of the axial frequency $\nu_{z,\mathrm{AT}}$. In the strong magnetic inhomogeneity, the orbital magnetic moment $\mu_+ = (q/m)(E_+/\omega_+)$ of the modified cyclotron mode is coupled to the axial frequency $\nu_{z,\mathrm{AT}}$, which becomes

$$\nu_{z,\mathrm{AT}} = \nu_{z,0,\mathrm{AT}} + \frac{1}{4\pi^2 m \nu_{z,0,\mathrm{AT}}} \frac{B_{2,\mathrm{AT}}}{B_{0,\mathrm{AT}}} E_+, \tag{2}$$

where $\nu_{z,0,\mathrm{AT}} \approx 657.92(1)$ kHz. For the parameters of our trap, the magnetic bottle shifts the axial frequency $\nu_{z,\mathrm{AT}}$ of a single trapped (anti)proton by $(1/k_\mathrm{B})(d\nu_{z,\mathrm{AT}}/dT_+) = 69.7(5)$ Hz per 1 K energy equivalent in the modified cyclotron mode, corresponding to an E_+ energy resolution of 14.7 mK, or 1.2 μeV per 1 Hz axial frequency shift.

To determine the axial frequency $\nu_{z,\mathrm{AT}}$ of the trapped antiproton in the analysis trap, a superconducting detection system with a quality factor of about $Q_\mathrm{AT} \approx 21\,500$, a detection inductance $L_\mathrm{AT} \approx 1.7$ mH, and a signal-to-noise ratio of 27 dB is used [27]. Appropriate adjustment of the voltages applied to the trap electrodes tunes the particles to resonance with the axial detector. In thermal equilibrium with the detection system, the particle shorts the thermal noise of the device at the particle's resonance frequency [25], and the axial frequency $\nu_{z,\mathrm{AT}}$ is determined by fitting a well-understood resonance line to the fast Fourier transform (FFT) of the recorded time-transient signal.

An important factor for the execution of efficient subthermal cooling protocols is the optimization of the time that is required to determine $\nu_{z,\mathrm{AT}}$. To efficiently sample axial frequencies, we subtract detector reference shots with 800 Hz bandwidth from spectra that include particle signatures [25], and identify those using peak threshold detection. The selected frequency window of 800 Hz covers an equivalent E_+/k_B-temperature range of ≈12 K, sufficient to resolve measured E_+ distributions at appropriate resolution. By tuning the trap parameters such that cold particles appear within the 3 dB width of the detection resonator, within a spectrum averaging time of ≈10 s particles with energies $E_+ < 440$ mK can be identified with better than 2σ detection significance.

For the preparation of a particle with low modified cyclotron energy E_+, we first prepare a single particle in the AT, and cool its magnetron mode to an energy of $E_-/k_\mathrm{B} = T_- < 7(1)$ mK, using magnetron-to-axial mode coupling techniques as the ones described in [28–30]. Subsequently, we apply the scheme illustrated in Fig. 2. First, we determine the particle's axial frequency by recording a single 12 s detector FFT spectrum as explained above. Next, by applying voltage ramps to 10 electrodes that connect the traps, the particle is shuttled from the AT to the CT. One transport takes 4.8 s, currently limited by the time constants of filters that connect the voltage supply lines to the trap electrodes. The used transport routines induce a scatter of about 14(2) cyclotron quanta per

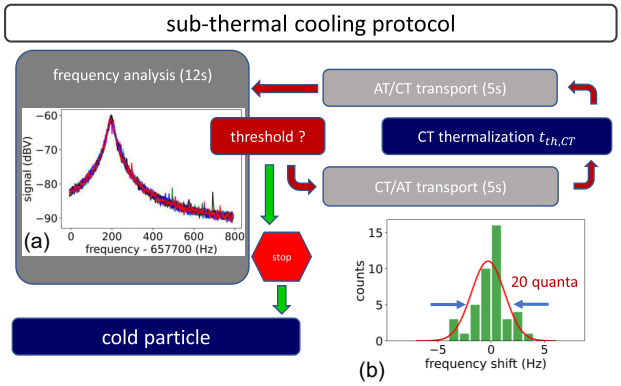

FIG. 2. Flowchart of the subthermal cooling protocol that is described in detail in the text. We cycle frequency measurements, particle transports, and particle thermalization in the CT until a threshold energy $E_{+,\mathrm{th}}$ is reached. For energies $E_+ < E_{+,\mathrm{th}}$ the sequence is stopped. (a) Illustrates axial resonator spectra, the peak features are signatures of particles at different E_+, we tune the trap such that a particle with vanishing cyclotron temperature would appear at the resonant center of the detector (200 Hz on the frequency axis). (b) Illustrates the measured trap-to-trap transport scatter, which is for AT → CT → AT at 20 cyclotron quanta per attempt.

executed transport protocol, see left lower inset in Fig. 2. This induces in temperature determinations a fluctuation background of 18 mK (≈1.2 Hz), negligibly small compared to the several 100 Hz fluctuations that need to be resolved. Subsequently, the particle is brought for a time $t_\mathrm{th,CT}$ in contact with the radial thermalization resistor $R_{p,\mathrm{CT}}$ in the CT. Using the varactor [18], the resonance frequency of this device is tuned to the CT modified cyclotron frequency, that was earlier determined by single particle cyclotron resonance spectroscopy [30]. Next, the particle is shuttled back to the AT, and its axial frequency is determined again. Following this protocol, one thermalization cycle requires about 22 s of frequency measurement and particle shuttling time, as well as the time $t_\mathrm{th,CT}$ for thermalization of the modified cyclotron mode in the CT. In contact with $R_{p,\mathrm{CT}}$, the particle's modified cyclotron mode is performing a random walk in E_+ energy space, once decoupled from the thermal bath, the walk "freezes" at a modified cyclotron energy $E_{+,\mathrm{CT},k}$, and reaches the AT with a radial orbital magnetic moment $\mu_{+,k}(E_+) = (q_0 E_{+,k})/(2\pi m_p \nu_+)$, inducing the E_+ dependent axial frequency shift given in Eq. (2). From experiments where $t_\mathrm{th,CT} = 20$ s was used, we obtain the AT axial frequencies shown in Fig. 3(a). These data represent an ≈12 K truncated Boltzmann distribution of a weakly bound one-dimensional thermalized oscillator. To determine the mean temperature of the particle's modified cyclotron mode after thermalization in the CT, and hence the temperature of the thermalization resistor $R_{P,\mathrm{CT}}$, we determine the lowest found frequency, use Eq. (2) and the measured $B_{2,\mathrm{AT}} \approx 266(8)$ kT/m^2 to scale the measured

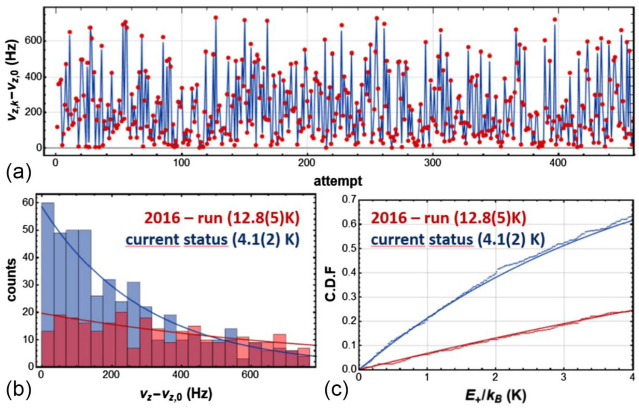

FIG. 3. (a) Frequencies measured in the AT within the subthermal cooling procedure at $T_+ = 4.1(2)$ K, recorded with the AT + CT double trap system described in this manuscript. (b) Data shown in (a) plotted to a histogram (blue), and compared to measurements performed with an earlier version of the apparatus. (c) Cumulative density functions of the results shown in (a).

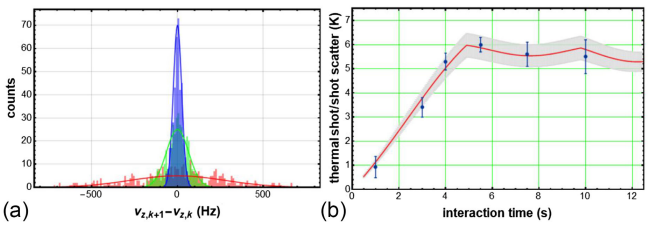

FIG. 4. (a) Histograms measured frequency differences $\nu_{z,\mathrm{AT},k+1} - \nu_{z,\mathrm{AT},k}$ for different particle/$R_{p,\mathrm{CT}}$ interaction times, blue 0.5 s, green 3 s, and red 15 s. (b) Widths of the histograms shown in (a) as a function of interaction time t_{th} in the CT.

frequency shifts $\Delta\nu_{z,k}$ to equivalent absolute temperatures T_k. Then we determine the number of measured events N_j in temperature intervals $\Delta T_+ = 0.001$ K, throughout the covered temperature range, and evaluate the normalized cumulative density function $\mathrm{CDF}(T_{\mathrm{thr}}) = 1/N_0 \cdot \sum_j^{N(T_{\mathrm{thr}})} N_j(\Delta T_+)$, where N_0 is the number of executed thermalization cycles and the index $N(T_{\mathrm{thr}})$ is defined by the threshold temperature T_{thr}. We fit to the resulting data the thermal cumulative density function $\mathrm{CDF}(T_{+,\mathrm{CT}}) = [(1 - \exp(-T/T_{+,\mathrm{CT}})]$, from which we extract the temperature of the thermalization resistor $T_{+,\mathrm{CT}} = 4.1(2)$ K. Figures 3(b) and 3(c) show results of this data treatment, blue for the current experiment, and red for thermalization in an apparatus without the cooling trap, where $E_+ = 12.8(5)$ K was measured [16]. For fully optimized parameters, the accumulation of the data set shown in Fig. 3 requires 3.7 h, whereas acquisition of the data set without cooling trap and optimized transport and readout procedures took 55 h. We account the threefold reduction in the temperature of $R_{P,\mathrm{CT}}$ to the relocation of the detection resistor closer to the trap, added cryogenic shielding and capacitive decoupling of the radio-frequency particle manipulation lines.

To investigate and optimize the limits of particle-detector interaction time t_{th}, we vary t_{th} in the CT, and measure the frequency scatter between the determined axial frequencies $\nu_{z,\mathrm{AT},k}$ before the thermalization and $\nu_{z,\mathrm{AT},k+1}$ afterward. Illustrated in Fig. 4(a), the width of frequency scatter histograms increases linearly with t_{th}, consistent with Monte Carlo simulations of the expected random-walk dynamics. Once the correlation time $\tau_{+,\mathrm{CT}}$ is reached, the widths of the measured frequency scatter histograms converge to a mean value, weakly $\tau_{+,\mathrm{CT}}$ structured by the correlation time of the thermalization of E_+. This behavior is shown in Fig. 4(b) for the particle parked in the center of the segmented electrode, which is the closest possible distance between particle and detection electrode, and provides the strongest particle-detector coupling. From these measurements we determine $\tau_{+,\mathrm{CT}} = 4.7(4)$ s, within uncertainties in perfect agreement with the theoretically expected $\tau_{+,\mathrm{CT,D}} = 4.5(2)$ s.

Applying this CT-based optimized Maxwell-daemon-cooling protocol, we achieve for single trapped protons and antiprotons cyclotron-mode energies $E_+/k_B < 200$ mK, at a particle preparation time of ≈500 s, which is about 80× faster than in our previous experiment, and corresponds to the fastest subthermal resistive cooling of a single particle in a Penning trap that has ever been demonstrated.

We apply our cooling scheme, to demonstrate nondestructive high-fidelity quantum jump spectroscopy with a single antiproton spin using the continuous Stern-Gerlach effect. The strong magnetic bottle $B_{2,\mathrm{AT}}$ of the AT couples the spin magnetic moment $\mu_{\bar{p}}$ to the axial frequency $\nu_{z,\mathrm{AT}} = \nu_{z,0,\mathrm{AT}} \pm \Delta\nu_{z,\mathrm{SF}}/2$, where $\nu_{z,0,\mathrm{AT}}$ is the axial frequency without spin, and $\Delta\nu_{z,\mathrm{SF}} = (\mu_{\bar{p}} B_{2,\mathrm{AT}})/(m_{\bar{p}}\nu_{z,0,\mathrm{AT}}) = 173$ mHz is the axial frequency shift induced by a spin transition. Performing such experiments with protons (p) and antiprotons $\bar{p}$ is outstandingly challenging, due to the small magnetic moments $\mu_{p,\bar{p}}$ and the comparably large mass $m_{p,\bar{p}}$ [19,31]. Quantum transitions $\Delta n_+ = \pm 65$ mHz in the modified cyclotron mode E_+, driven by tiny noise densities on the trap electrodes [17], lead to axial frequency fluctuations, and therefore to considerable error rates in the spin state identification protocols that are applied in Penning trap based measurements of $\mu_{p,\bar{p}}$. The heating rates dn_+/dt scale however $\propto E_+$ [32], such that for colder particles the contrast in the spin state identification increases. We apply the subthermal cooling protocol and prepare a single antiproton at $E_+/k_B < 100$ mK in the center of the AT. Thanks to the cooling trap, preparing such a particle takes < 20 min. Subsequently, we apply a sequence of axial frequency $\nu_{z,\mathrm{AT}}$ measurements, interleaved with resonant saturated spin-flip drives that incoherently invert the spin state in the AT [33]. Results of these measurements are

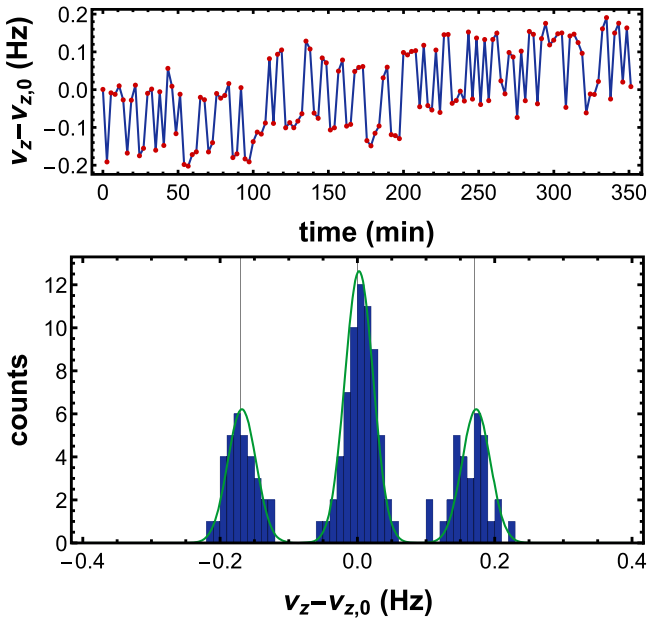

FIG. 5. Top: axial frequency of a single trapped antiproton in the AT, between two subsequent $\nu_{z,\mathrm{AT}}$ measurements a resonant saturating spin flip drive is applied. Bottom: histogram of measured axial frequency differences $\nu_{z,k+1,\mathrm{AT}} - \nu_{z,k,\mathrm{AT}}$. The left-right part of the histogram represents a $|\uparrow\rangle \to |\downarrow\rangle/|\downarrow\rangle \to |\uparrow\rangle$ transition, for the central historgram the antiproton spin was not inverted. The rms widths of the histograms are consistent with the stability of the power supply that biases the trap electrodes of the AT.

shown in Fig. 5, the upper plot displays the measured frequencies $\nu_{z,\mathrm{AT}}$, the two antiproton spin quantum states $|\downarrow\rangle$ and $|\uparrow\rangle$ can be clearly distinguished. The lower histogram shows the measured frequency differences $\nu_{z,k+1,\mathrm{AT}} - \nu_{z,k,\mathrm{AT}}$ plotted to a histogram. The subhistograms at $\Delta\nu_{z,AT} = \pm 173(1)$ mHz represent transitions $|\uparrow\rangle \to |\downarrow\rangle/|\downarrow\rangle \to |\uparrow\rangle$ respectively, for the central histogram, the antiproton spin was not inverted. The rms widths of the histograms $\sigma(\nu_{z,\mathrm{AT}}) = 21(1)$ mHz are consistent with power-supply and detector-based frequency measurement noise. The error rate E_S—the probability to incorrectly assign an observed frequency shift $\Delta\nu_z$ to a spin transition, given a defined detection threshold Δ_{TH}—is at that performance of the experiment at a level of 2.3×10^{-5}, which corresponds to a $> 1500\times$ improvement compared to the previous best reported E_S [22]. The cooling trap allows us to achieve such low spin-state-detection error rates almost $100\times$ faster than in [16], allowing for experiments at much improved antiproton magnetic moment sampling rates, impacting future measurement precision and time resolution of studies of exotic physics [11,34]. Our development also opens perspective toward direct magnetic moment measurements of heavier nuclei, such as $^3He^{2+}$, to establish a new standard for absolute magnetometry [2]. Another application of the cooling presented here are coherent measurements of cyclotron frequencies in high-precision mass spectrometry and measurements of the bound electron g factor [14]. In those experiments, sideband-cooling techniques are applied, that lead to mode-temperature related phase scatter, which could be considerably suppressed by applying the above cooling-trap technique.

We acknowledge financial support by RIKEN, the Max-Planck Society, CERN, Heinrich Heine University Duesseldorf, the European Union (FunI-832848, STEP-852818), CRC 1227 "DQ-mat"(DFG 274200144), the Cluster of Excellence "Quantum Frontiers" (DFG 390837967), the Wolfgang Gentner Program (Grant No. 13E18CHA), IMPRS-QD, and the Helmholtz-Gemeinschaft. This work was supported by the Max-Planck, RIKEN, PTB-Center for Time, Constants, and Fundamental Symmetries (C-TCFS).

[1] E. G. Myers, High-precision atomic mass measurements for fundamental constants, Atoms **7**, 37 (2019).
[2] G. Schneider, A. Mooser, M. Bohman, N. Schön, J. Harrington, T. Higuchi, H. Nagahama, S. Sellner, C. Smorra, K. Blaum *et al.*, Double-trap measurement of the proton magnetic moment at 0.3 parts per billion precision, Science **358**, 1081 (2017).
[3] D. Hanneke, S. Fogwell, and G. Gabrielse, New measurement of the electron magnetic moment and the fine structure constant, Phys. Rev. Lett. **100**, 120801 (2008).
[4] R. S. Van Dyck Jr, P. B. Schwinberg, and H. G. Dehmelt, New high-precision comparison of electron and positron g factors, Phys. Rev. Lett. **59**, 26 (1987).
[5] M. Borchert, J. Devlin, S. Erlewein, M. Fleck, J. Harrington, T. Higuchi, B. Latacz, F. Voelksen, E. Wursten, F. Abbass *et al.*, A 16-parts-per-trillion measurement of the antiproton-to-proton charge–mass ratio, Nature (London) **601**, 53 (2022).
[6] A. Schneider, B. Sikora, S. Dickopf, M. Müller, N. Oreshkina, A. Rischka, I. Valuev, S. Ulmer, J. Walz, Z. Harman *et al.*, Direct measurement of the $^3He^+$ magnetic moments, Nature (London) **606**, 878 (2022).
[7] X. Fan, T. G. Myers, B. A. D. Sukra, and G. Gabrielse, Measurement of the electron magnetic moment, Phys. Rev. Lett. **130**, 071801 (2023).
[8] K. Blaum, S. Eliseev, and S. Sturm, Perspectives on testing fundamental physics with highly charged ions in Penning traps, Quantum Sci. Technol. **6**, 014002 (2020).
[9] T. Sailer, V. Debierre, Z. Harman, F. Heiße, C. König, J. Morgner, B. Tu, A. V. Volotka, C. H. Keitel, K. Blaum *et al.*, Measurement of the bound-electron g-factor difference in coupled ions, Nature (London) **606**, 479 (2022).
[10] S. Eliseev, K. Blaum, M. Block, S. Chenmarev, H. Dorrer, C. E. Düllmann, C. Enss, P. E. Filianin, L. Gastaldo, M. Goncharov *et al.*, Direct measurement of the mass difference of ^{163}Ho and ^{163}Dy solves the Q-value puzzle for the neutrino mass determination, Phys. Rev. Lett. **115**, 062501 (2015).

[11] C. Smorra, Y. Stadnik, P. Blessing, M. Bohman, M. Borchert, J. Devlin, S. Erlewein, J. Harrington, T. Higuchi, A. Mooser *et al.*, Direct limits on the interaction of antiprotons with axion-like dark matter, Nature (London) **575**, 310 (2019).

[12] J. Ketter, T. Eronen, M. Höcker, M. Schuh, S. Streubel, and K. Blaum, Classical calculation of relativistic frequency-shifts in an ideal Penning trap, Int. J. Mass Spectrom. **361**, 34 (2014).

[13] F. Heiße, F. Köhler-Langes, S. Rau, J. Hou, S. Junck, A. Kracke, A. Mooser, W. Quint, S. Ulmer, G. Werth *et al.*, High-precision measurement of the proton's atomic mass, Phys. Rev. Lett. **119**, 033001 (2017).

[14] S. Sturm, F. Köhler, J. Zatorski, A. Wagner, Z. Harman, G. Werth, W. Quint, C. H. Keitel, and K. Blaum, High-precision measurement of the atomic mass of the electron, Nature (London) **506**, 467 (2014).

[15] M. J. Borchert, Challenging the Standard Model by high precision comparisons of the fundamental properties of antiprotons and protons, Institutionelles Repositorium der Leibniz Universität Hannover, Hannover, 2021.

[16] C. Smorra, S. Sellner, M. Borchert, J. Harrington, T. Higuchi, H. Nagahama, T. Tanaka, A. Mooser, G. Schneider, M. Bohman *et al.*, A parts-per-billion measurement of the antiproton magnetic moment, Nature (London) **550**, 371 (2017).

[17] M. J. Borchert, P. E. Blessing, J. A. Devlin, J. A. Harrington, T. Higuchi, J. Morgner, C. Smorra, E. Wursten, M. Bohman, M. Wiesinger *et al.*, Measurement of ultralow heating rates of a single antiproton in a cryogenic Penning trap, Phys. Rev. Lett. **122**, 043201 (2019).

[18] S. Ulmer, K. Blaum, H. Kracke, A. Mooser, W. Quint, C. C. Rodegheri, and J. Walz, A cryogenic detection system at 28.9 MHz for the non-destructive observation of a single proton at low particle energy, Nucl. Instrum. Methods Phys. Res., Sect. A **705**, 55 (2013).

[19] S. Ulmer, C. C. Rodegheri, K. Blaum, H. Kracke, A. Mooser, W. Quint, and J. Walz, Observation of spin flips with a single trapped proton, Phys. Rev. Lett. **106**, 253001 (2011).

[20] C. Smorra, A. Mooser, M. Besirli, M. Bohman, M. J. Borchert, J. Harrington, T. Higuchi, H. Nagahama, G. L. Schneider, S. Sellner, T. Tanaka, K. Blaum, Y. Matsuda, C. Ospelkaus, W. Quint, J. Walz, Y. Yamazaki, and S. Ulmer, Observation of individual spin quantum transitions of a single antiproton, Phys. Lett. B **769**, 1 (2017).

[21] S. Sellner, M. Besirli, M. Bohman, M. Borchert, J. Harrington, T. Higuchi, A. Mooser, H. Nagahama, G. Schneider, C. Smorra *et al.*, Improved limit on the directly measured antiproton lifetime, New J. Phys. **19**, 083023 (2017).

[22] C. Smorra *et al.*, BASE—The Baryon Antibaryon Symmetry Experiment, Eur. Phys. J. Special Topics **224**, 3055 (2015).

[23] G. Gabrielse, L. Haarsma, and S. Rolston, Open-endcap Penning traps for high precision experiments, Int. J. Mass Spectrom. Ion Process. **88**, 319 (1989).

[24] W. Macalpine and R. Schildknecht, Coaxial resonators with helical inner conductor, Proc. IRE **47**, 2099 (1959).

[25] D. Wineland and H. Dehmelt, Principles of the stored ion calorimeter, J. Appl. Phys. **46**, 919 (1975).

[26] G. Gabrielse, A. Khabbaz, D. S. Hall, C. Heimann, H. Kalinowsky, and W. Jhe, Precision mass spectroscopy of the antiproton and proton using simultaneously trapped particles, Phys. Rev. Lett. **82**, 3198 (1999).

[27] H. Nagahama, G. Schneider, A. Mooser, C. Smorra, S. Sellner, J. Harrington, T. Higuchi, M. Borchert, T. Tanaka, M. Besirli *et al.*, Highly sensitive superconducting circuits at 700 kHz with tunable quality factors for image-current detection of single trapped antiprotons, Rev. Sci. Instrum. **87**, 113305 (2016).

[28] E. A. Cornell, R. M. Weisskoff, K. R. Boyce, and D. E. Pritchard, Mode coupling in a Penning trap: π pulses and a classical avoided crossing, Phys. Rev. A **41**, 312 (1990).

[29] N. Guise, J. DiSciacca, and G. Gabrielse, Self-excitation and feedback cooling of an isolated proton, Phys. Rev. Lett. **104**, 143001 (2010).

[30] H. Nagahama, C. Smorra, S. Sellner, J. Harrington, T. Higuchi, M. Borchert, T. Tanaka, M. Besirli, A. Mooser, G. Schneider *et al.*, Sixfold improved single particle measurement of the magnetic moment of the antiproton, Nat. Commun. **8**, 14084 (2017).

[31] H. Dehmelt, Continuous Stern-Gerlach effect: Principle and idealized apparatus, Proc. Natl. Acad. Sci. U.S.A. **83**, 2291 (1986).

[32] A. Mooser, H. Kracke, K. Blaum, S. A. Bräuninger, K. Franke, C. Leiteritz, W. Quint, C. C. Rodegheri, S. Ulmer, and J. Walz, Resolution of single spin flips of a single proton, Phys. Rev. Lett. **110**, 140405 (2013).

[33] L. S. Brown and G. Gabrielse, Geonium theory: Physics of a single electron or ion in a Penning trap, Rev. Mod. Phys. **58**, 233 (1986).

[34] D. Budker, P. W. Graham, H. Ramani, F. Schmidt-Kaler, C. Smorra, and S. Ulmer, Millicharged dark matter detection with ion traps, PRX Quantum **3**, 010330 (2022).